



## Glacier evolution in high mountain Asia under stratospheric sulfate aerosol injection geoengineering

Liyun Zhao<sup>1,2</sup>, Yang Yi<sup>1</sup>, Duoying Ji<sup>1,2</sup>, John C. Moore<sup>1,2,3</sup>

<sup>1</sup>College of Global Change and Earth System Science, Beijing Normal University,  
5 19 Xijiekou Wai St., Beijing, 100875, China

<sup>2</sup>Joint Center for Global Change Studies, Beijing, 100875, China

<sup>3</sup>Arctic Centre, University of Lapland, P.O. Box 122, 96101 Rovaniemi, Finland

Corresponding author: john.moore.bnu@gmail.com

### 10 **Abstract:**

Geoengineering by stratospheric sulfate aerosol injection may help preserve mountain  
glaciers by reducing summer temperatures. We examine this hypothesis for the glaciers  
in High Mountain Asia using a glacier mass balance model driven by climate  
simulations from the Geoengineering Model Intercomparison Project (GeoMIP). The  
15 G3 and G4 schemes specify use of stratospheric sulphate aerosols to reduce the  
radiative forcing under the Representative Concentration Pathway (RCP) 4.5 scenario  
for the 50 years between 2020 and 2069, and for a further 20 years after termination of  
geoengineering. We estimate and compare glaciers volume loss for every glacier in the  
region using a model based on glacier surface mass balance parameterization under  
20 climate projections from 3 Earth System Models under G3, 5 under G4 and 6 under  
RCP4.5 and RCP8.5. G3 keeps the summer mean temperature from increasing in the  
geoengineering period, but termination of geoengineering leads to sudden temperature  
rise of about 1.7° C and corresponding increase in glacier retreat. Glacier volume in  
inner Tibet and eastern Himalaya is least affected by greenhouse gas forcing, and also  
25 benefits the most from geoengineering. The ensemble mean projections suggest that  
glacier shrinkage over the period 2010-2069 are equivalent to sea-level rises of 8.4 mm  
(G3), 10.7 mm (G4), 14.7 mm (RCP 4.5) and 16.8 mm (RCP8.5). After the termination  
of geoengineering, annual mean volume loss rate for all the glaciers under G3 increases  
from 0.39% a<sup>-1</sup> to 0.90% a<sup>-1</sup>, which are higher than the 0.70% a<sup>-1</sup> under RCP8.5 at that



30 time. While sulphate aerosol injection geoengineering may slow glacier loss in the  
region, it cannot prevent about a third of existing glacier coverage disappearing by 2069.

**keywords:** sea level rise; mass balance; climate impacts

## 35 1. Introduction

High Mountain Asia (HMA) contains the largest number of glaciers outside the polar  
regions. These glaciers provide water for many large and important rivers (e.g.  
Brahmaputra, Ganges, Yellow, Yangtze, Indus, and Mekong), and most, but not all,  
have shrunk over recent decades (Yao et al., 2012). The response of these glaciers to  
40 future climate change is a topic of concern especially to the many people who rely on  
glacier-fed rivers for purposes such as irrigation.

Glacier evolution is expected to be sensitive to climate change. Temperature and  
precipitation are the important climate factors affecting glaciers. Geoengineering is a  
method of offsetting the global temperature rise from greenhouse gases, although  
45 inevitably also altering other important climate parameters, such as precipitation and  
global atmosphere and ocean circulation teleconnection patterns (Tilmes, et al., 2013;  
Ricke, et al., 2010). There have been various studies on mountain glacier change under  
future climate scenarios such as A1B, and the various Representative Concentration  
Pathway (RCP) scenarios (Marzeion et al., 2012; Radić et al., 2014; Zhao et al., 2014).  
50 In contrast to glaciers in higher latitudes, those in HMA are mainly summer  
accumulation type, that is both surface snow fall and melting occur overwhelmingly in  
the 3 summer months of June, July and August, with little mass gain or loss throughout  
the remaining 9 months of the year. The glaciers are affected by both the South Asian  
monsoon system and the westerly cyclonic systems, depending on specific location  
55 across the region. Hence the region is important both to people dependent on glacier  
water supplies, and because it integrates the climate response to important global  
circulation systems. However, glacier responses to geoengineering scenarios has been  
limited to studies on global responses based on semi-empirical models (Moore et al.,  
2010) or from simplified ice sheet responses (Irvine et al. 2009, 2012; McCusker et al.,  
60 2015; Applegate et al., 2015), with nothing to date on mountain glacier impacts.



In this paper, we predict glacier area and volume change for every glacier in HMA under forcing by output from 6 Earth System Models (ESM) simulations of climate under the Geoengineering Model Intercomparison Project (GeoMIP) G3 and G4 scenarios (Kravitz et al., 2011). These scenarios envisage use of stratospheric sulphate aerosols to reduce the radiative forcing under the RCP 4.5 greenhouse gas scenario during in a 50 year period from 2020 to 2069 followed by sudden cessation of geoengineering to determine the “termination effect” (Jones et al., 2013) but continued RCP4.5 greenhouse gas forcing for a further 20 years. We address two questions here: (1) Would glacier shrinkage and loss in HMA be alleviated under geoengineering by stratospheric sulfate aerosol injection? (2) How would the glaciers respond to the termination of geoengineering?

## 2. Study region and glacier data

Our study region covers HMA (26–46° N, 65–105° E), which corresponds to the regions of newly defined regions of Central Asia, South Asia West and South Asia East in the Randolph Glacier Inventory (RGI) 5.0 (Arendt et al., 2015). According to the RGI5.0, the study region contains a total of 94,000 glaciers and a glaciated area of about 110,000 km<sup>2</sup>. To estimate how each of these glaciers change we require for each one a reference area and volume. Glacier area estimates inside China are based on the Second Chinese Glacier Inventory (Guo et al., 2015), which provides glacier outlines from a target period of 2006–2010, but includes older outlines from the First Chinese Glacier Inventory where suitable imagery could not be found within the target period - mainly in the southern and eastern Tibet sub-region. Glacier outlines outside China are from the “Glacier Area Mapping for Discharge from the Asian Mountains” (GAMDAM) inventory (Nuimura et al., 2015) and nearly all come from 1999–2003 with images selected as close to the year 2000 as possible. Therefore, for simplicity, we take 1980, 2009 and 2000 as the reference years and start of our model simulations for glaciers inside southern and eastern Tibet, inside China except southern and eastern Tibet, and outside China, respectively.



90 We use median altitude from RGI 5.0 for each glacier as a proxy for equilibrium line  
altitude (ELA) in the respective initial years; that is the altitude on the glacier where the  
local net surface mass balance (SMB) is zero. We use the Shuttle Radar Topography  
Mission (SRTM) version 4.1 (void-filled version; Jarvis et al, 2008) digital elevation  
95 glacier.

Field measurements on SMB are rare in the HMA due to difficulty of access to the  
glaciers. Here we collate SMB versus altitude measurements from 13 glaciers (Table 1  
and Fig. 1), to set up parameterizations of mass balance with altitude relative to the  
ELA for all glaciers. This field data are more than previously used in the model (Zhao  
100 et al., 2014; 2016), with a benchmark glacier in almost every sub-regions. With so few  
glacier observations available there is an issue of how representative they are of the  
general population. For inner Tibet, there are 3 glaciers (Zhadang, Gurenhekou and  
Xiao Dongkemadi Glacier) with SMB observations, and they have almost the same  
value of SMB gradients in similar altitude ranges (Table 1); as so do the two glaciers  
105 (Naimona'nyi and Kangwure) in central Himalaya. These similarities suggest that at  
least the measured glaciers share some important characteristics with the vast majority  
which are not surveyed.

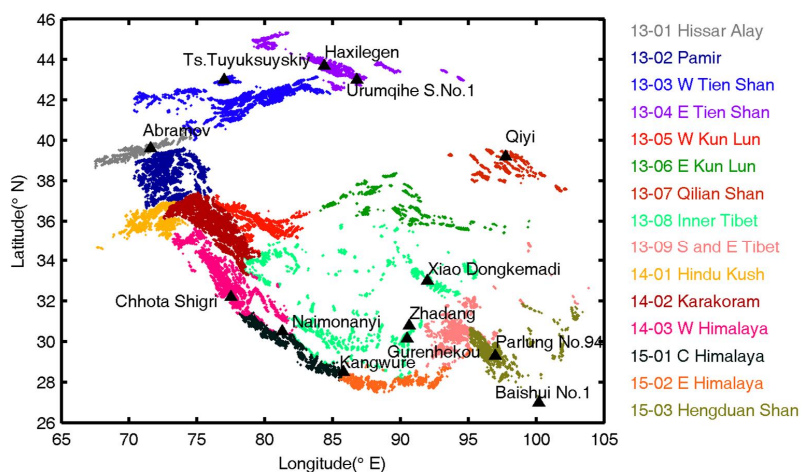


Fig. 1 The HMA region analyzed. Sub-regions of the HMA in RGI 5.0 are listed and  
110 colour-coded in the legend. The black curves represent the boundaries between regions



13 (Central Asia), 14 (South Asia West) and 15 (South Asia East). Glaciers with SMB measurements (Table 1) are marked with black triangles.

### 3. Methodology

#### 115 3.1 Statistical model of glacier change

The statistical model for estimating glacier change is based on Zhao et al (2014; 2016). Briefly the algorithm can be described as follows. We start from known glacier outlines from RGI 5.0 and glacier elevation distribution from SRTM 4.1. We parameterize the annual SMB as a function of altitude relative to the ELA for each glacier. We use the available SMB measurements on 13 glaciers (Fig. 1) to calculate two or three SMB  
120 gradients with altitude (Table 1). The SMB–altitude profile is constructed for every glacier by using its own ELA and no more than three SMB gradients. Where SMB data exists in the sub-region we use them to parameterize the SMB of all glaciers in that sub-region. Otherwise, we use glaciers from nearby sub-regions. Integrating the SMB over  
125 each glacier gives the volume change rate, which is converted to an area change rate using volume–area scaling. The area change rate then gives the new glacier terminus position and hence the new outline for the next year by assuming all the decrease in area takes place in the lowest parts of the glacier. Combining the glacier elevation distribution, the SMB and the new outline, we obtain glacier elevation distribution for  
130 the next year.

The SMB–altitude profile on each glacier is evolved annually as the ELA changes. And the ELA evolution is estimated by using its sensitivities with respect to temperature and precipitation as follows:

$$ELA_n = ELA_{n-1} + \alpha \Delta T + \beta \Delta P, \quad (1)$$

135 where  $ELA_n$  is the ELA in the  $n^{\text{th}}$  year from the beginning year,  $\Delta T$  and  $\Delta P$  are the inter-annual change of summertime (June-July-August) mean air temperature and annual precipitation, the coefficients  $\alpha$  (unit:  $\text{m } ^\circ\text{C}^{-1}$ ) and  $\beta$  (unit:  $\text{m } \text{m}^{-1}$ ) are the sensitivity of ELA shift to air temperature change ( $^\circ\text{C}$ ) and precipitation change (m), respectively, which are zonal mean values from energy-balance modelling of glaciers



140 in HMA by Rupper and Roe (2008), see also Zhao et al. (2014). We show in Section 4,  
that simulated precipitation changes under all the climates we study here are relatively  
small (<10%). Therefore we choose to remove precipitation changes from our  
simulations of HMA glaciers, hence we assume that changes of ELA in Eqn (1) are  
controlled by summer temperature variation alone.

145

### 3.2 Climate scenarios and downscaling of climate data

We run the simulations for glacier change from the relevant start years (Section 2) to  
the year 2089. From the beginning years to 2013, we use the relatively high resolution,  
daily gridded  $1^\circ \times 1^\circ$  temperature data from the Berkeley Earth project (Rohde et al.,  
150 2013; <http://berkeleyearth.org/data/>) which are generated by supposedly using all  
available station data and a bespoke interpolation method.

We use the Coupled Model Intercomparison Project Phase 5 (CMIP5; Taylor, et al.,  
2012) output of all models. For the years 2014 to 2089 we use 4 kinds of climate forcing:  
experiment RCP4.5, RCP8.5, and results from two GeoMIP scenarios (G3 and G4;  
155 Kravitz et al., 2011) which use stratospheric aerosols to reduce the incoming shortwave  
while applying the RCP4.5 greenhouse gas forcing. In G3 and G4, stratospheric  
geoengineering of sulphate aerosol injection starts in the year 2020 and ends in the year  
2069. In the 50 years of geoengineering under G3 there is close to a balance between  
reduction of incoming shortwave radiation and greenhouse gas forcing, while G4  
160 specifies continuous injection of  $\text{SO}_2$  into the equatorial lower stratosphere at a rate of  
5 Tg per year from 2020. Following the abrupt end of geoengineering, both G3 and G4  
specify 20 years of further simulation from 2070 to 2089 driven by forcing from  
RCP4.5 alone.

We derived climate forcing data from 3 climate models participating in G3, 5 in G4,  
165 6 in RCP4.5 and 6 in RCP8.5 (Table 2). Following Yu et al. (2015), we do not use any  
GISS-E2-R results here because its projected fields are very different from other models.  
We also exclude the model CISRO-Mk3L due to its very coarse resolution of about  $4^\circ$   
and the absence of simulation result in the year 2020 under G4; the models used and



their resolutions are listed in Table 2.

170 Compared with the size of most glaciers in HMA (typically km scale), both the  
Berkeley grids and climate models grids have rather coarse resolution. The direct use  
of coarse grid points naturally results in a poor representation of the local climate.  
Hence we downscale both the Berkeley gridded data and the climate models output to  
a grid based on a land surface topography having resolution of  $0.1126^\circ \times 0.1126^\circ$  using  
175 an altitude temperature lapse rate of  $0.65^\circ\text{C}/100\text{ m}$  and elevation difference of the fine  
grid relative to the climate model grid. For each individual glacier, we use the data at  
the grid nearest to this glacier to represent the local climate.

We bias correct the downscaled model temperatures output by using Berkeley  
gridded data as a reference climate. Downscaled series were produced for each  
180 climate model for the period 2013 to 2089 under each climate scenario by averaged  
monthly differences over the baseline period 1980 to 2005 taken from the CMIP5  
*historical* simulations of the models. We only use summer (JJA) mean near-surface  
air temperature. Therefore, future temperature time series  $T_i(t)$  on each grid were  
calculated by

$$185 \quad T_i(t) = T_{i,c}(t) + (\bar{T}_{i,Berkeley} - \bar{T}_{i,c,history}), \quad i = 6, 7, 8.$$

where  $T_{i,c}(t)$  is monthly mean temperature for the  $i$ th month from the climate model  
output from  $t = 2013$  to 2089,  $\bar{T}_{i,Berkeley}$  and  $\bar{T}_{i,c,history}$  are mean temperature from  
Berkeley Earth project and climate model output, respectively, for the  $i$ th month  
averaged over the baseline period 1980-2005 on each grid.

190

## 4. Results

### 4.1 Regional temperature and precipitation change

Using the downscaled climate data (section 3), we estimate the mean surface air  
temperature and precipitation anomalies during 2030-2069 simulated by the relevant  
195 model ensembles under G3, G4, RCP4.5 and RCP8.5 (Fig. 2 and Fig. 3). Over the  
period from 2030 to 2069, the regional average temperature increases moderately by



0.17 ± 0.18 °C under G3 compared with the baseline (taken as the ensemble mean of each model's RCP4.5 average over 2010–2029; Table 3). The temperature increases mainly over the north of the study region (including Tien Shan and Pamir). The regional average over 2030–2069 increases by 0.50 ± 0.34 °C under G4, and 1.30 ± 0.34 °C under RCP4.5 compared with the baseline. The ensemble mean temperature under G4 tends to decrease over the Himalayas, but with low model agreement.

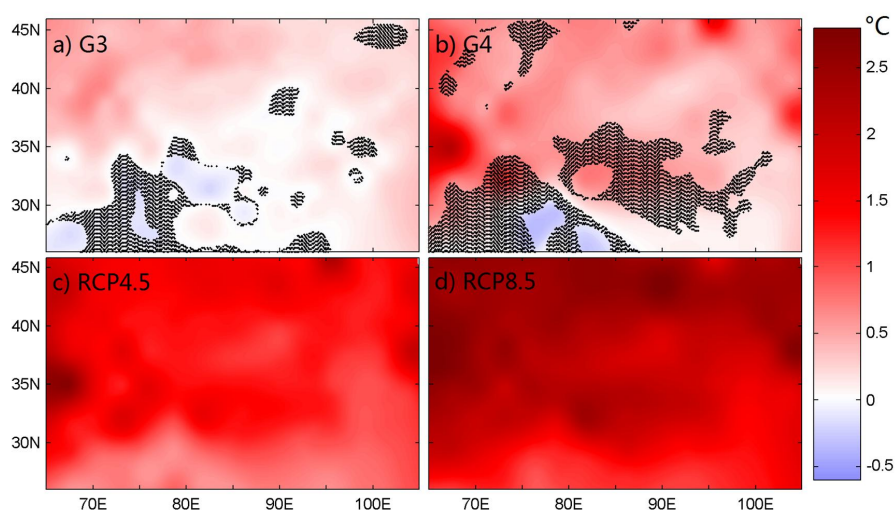
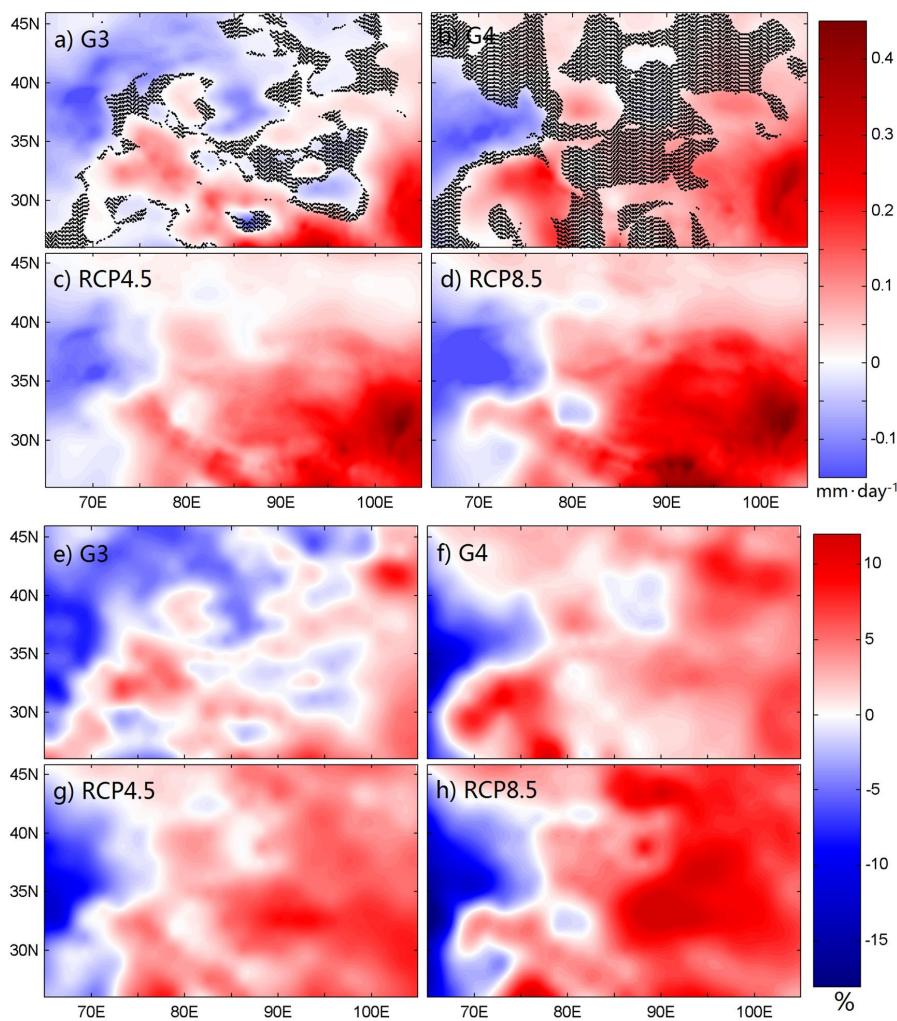


Fig 2. Ensemble mean surface air temperature anomalies during 2030–2069 simulated under G3 (a); G4 (b); RCP4.5 (c); RCP8.5 (d). The ensemble members are listed in Table 2. Anomalies are relative to the baseline RCP4.5 climate state between 2010 and 2029. Stippling indicates where fewer than 2/3 models agreed on the sign of change for (a), fewer than 4/5 models agreed for (b), fewer than 5/6 models agreed for (c) and (d).

Regional averaged precipitation under G4 and RCP4.5 between 2030 and 2069 are increased by 0.05 ± 0.08 mm day<sup>-1</sup> and 0.07 ± 0.10 mm day<sup>-1</sup>, respectively, compared with the baseline and slightly more for RCP8.5 (Table 3). The precipitation under G4 increases over most of the area but with low model agreement. The patterns of precipitation change under G4 are similar to those under RCP4.5 and RCP8.5. The precipitation anomaly value increases from west to east and reaches the maximum in the south east of the region. The ensemble mean of the regional average precipitation



change under G3 is negligible relative to the baseline, and the across-model variation is much larger than the ensemble mean. The precipitation change ratios under the 3 climate scenarios are from -15% to 10% (Fig. 3).



220

Fig 3. As that for Fig. 2 but for precipitation anomalies (a-d) and precipitation percentage change (e-h).

#### 4.2 Temperature forcing for glacier change

225 The across-region summer mean temperature projections ensembles under G3, G4, RCP4.5 and RCP8.5 are shown in Fig. 4. We use Berkeley gridded temperature before 2013 and ensemble means of climate models (Table 2) with model bias correction



(Section 3.2) under RCP4.5 from 2014 to 2019, and that under climate scenarios G3, G4, RCP4.5 and RCP8.5 from the year 2020 to 2089. We ensure that means of all ensembles at each grid point are equal at the year 2020. Figure 5 shows the time series of JJA mean temperature forcing from the beginning years to 2089. The temperature averages over the whole region and glaciated parts have similar trends.

Temperatures under RCP8.5 increase linearly and the highest rate among all the scenarios. Temperature increases under RCP4.5 are next, and its rate becomes smaller after about the year 2050 as specified greenhouse gas emissions decline. There is an obvious cooling effect (about  $0.75^{\circ}\text{C}$ ) projected by G4 compared with RCP4.5 during 2020-2069 over the whole region (Fig. 5). There is no trend in temperature under G3 in the geoengineering period (2020-2069). But after the termination in the year 2069, there is a temperature rise of about  $1.7^{\circ}\text{C}$  under G3. There is no similar termination rise under G4 where the temperature trend in the post-geoengineering period is almost the same as that earlier.

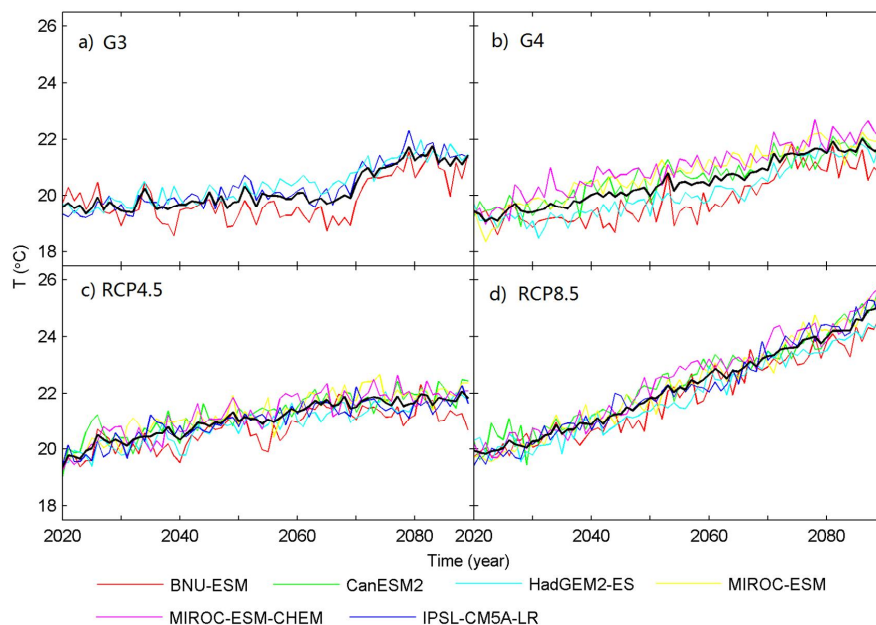
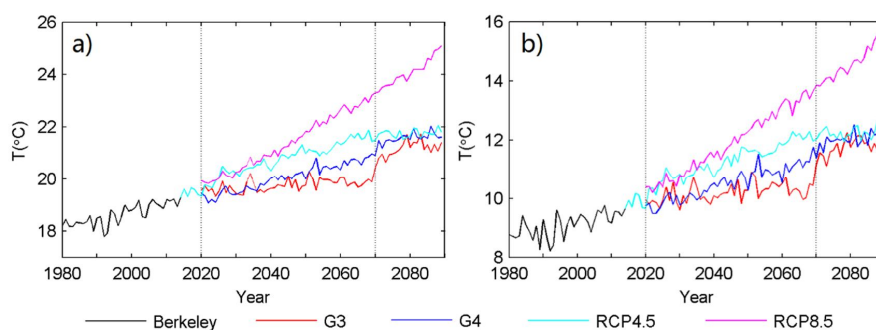


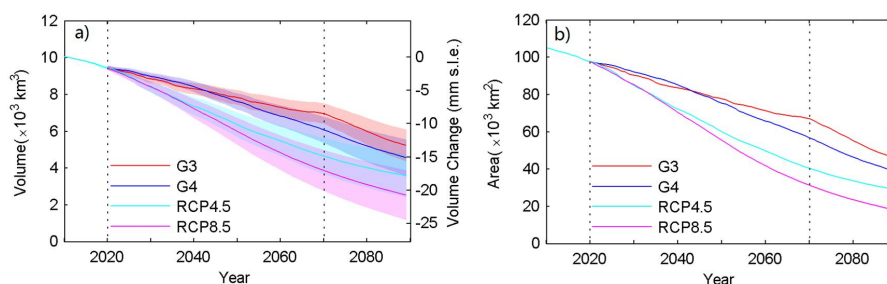
Fig. 4. Time series of summer mean temperature averaged over the grids in the whole region projected by ensemble members after model bias correction under climate



245 scenarios G3 (a), G4 (b), RCP4.5 (c) and RCP8.5 (d). Black curve in each plot is the  
mean of the ensemble.



250 Fig. 5. Time series of summer mean temperature averaged over the grids in the whole  
region (a) and only in the glaciated region (b). Note the different temperature ranges.



255 Fig. 6. Total glacier volume in HMA (a) and the equivalent sea level rise assuming an  
ice density of  $900 \text{ kg m}^{-3}$  and ocean area of  $362 \times 10^{12} \text{ m}^2$  and (b) area changes from  
2010 to 2089. Uncertainty in a) reflects factors in the statistical model discussed in  
section 4.3.

### 4.3 Glacier change

#### 4.3.1 Under different climate forcing

260 Glacier volume changes for all the glaciers in the study region computed using  
temperature data from the four scenarios are shown in Fig. 6a. Volume loss rates  
increase from G3, G4, RCP4.5 to RCP8.5 for the period 2020-2089. The RCP4.5 and  
RCP8.5 scenarios produce similar continuous mass loss until approximately 2035, and



both show relatively slower loss rates after about the year 2050. The glacier volume  
265 loss in equivalent to sea-level rise for the whole study region from 2010 to the end of  
geoengineering in 2069 is 8.4 mm (G3), 10.7 mm (G4), 14.7 mm (RCP 4.5) and 16.8  
mm (RCP8.5), with 93.3%, 95.7%, 99.4% and 100% glaciers retreating under these  
scenarios. Therefore, the geoengineering schemes G3 and G4 help to reduce glacier  
mass loss in our simulations, and G3 reduces glacier loss more than G4.

270 There is a clear increase in volume loss rate under G3 after 2069 when  
geoengineering is terminated. Comparing the last 15 years of geoengineering (2055-  
2069) with the first 15 years of post-geoengineering (2070-2084) shows annual mean  
volume loss rate for all the glaciers of  $0.39\% \text{ a}^{-1}$  (referenced to the volume in the year  
2010) increases to  $0.90\% \text{ a}^{-1}$ , which is higher than the rates of  $0.56\% \text{ a}^{-1}$  for RCP4.5  
275 and  $0.70\% \text{ a}^{-1}$  for RCP8.5. However, the volume loss rate under G4 shows negligible  
termination effect; annual mean volume loss rates change from  $0.73\% \text{ a}^{-1}$  to  $0.78\% \text{ a}^{-1}$   
before and after the termination. The glacier volume loss over the post geoengineering  
period of 2070-2089 for both G3 (4.8 mm) and G4 (4.1 mm) are higher than for either  
RCP 4.5 (3.0 mm) or RCP8.5 (3.7 mm). However, by 2070 under both RCP scenarios  
280 there is much less glacier ice volume remaining than under G4, or especially G3.  
Comparing ice loss rates at comparable total volumes, loss rates with RCP8.5 are  
similar to those of post geoengineering G3.

Glacier area change trends under each climate scenario are quite similar to the  
volume change trends (Fig. 6b). We project 44%, 37%, 28% and 17% of the area in  
285 2010 remaining in the year 2089 under the G3, G4, RCP 4.5 and RCP8.5 scenarios,  
respectively.

#### 4.3.2 Variations across sub-regions

Glacier volume changes in the HMA sub-regions are shown in Fig. 7. Glacier volumes  
290 in most sub-regions decrease for the whole period, with the highest rates under RCP8.5  
and lowest under G3, as expected. Glacier volume in inner Tibet under G3, and in  
eastern Himalaya under both G3 and G4 are unchanging or slightly increasing in the  
geoengineering period 2020-2069, because the summer mean air temperature has no



trend there. The “termination effect” of geoengineering under G3 is significant in most  
 295 sub-regions. However, there is no obvious change in glacier volume loss rate before  
 and after 2070 under G4.

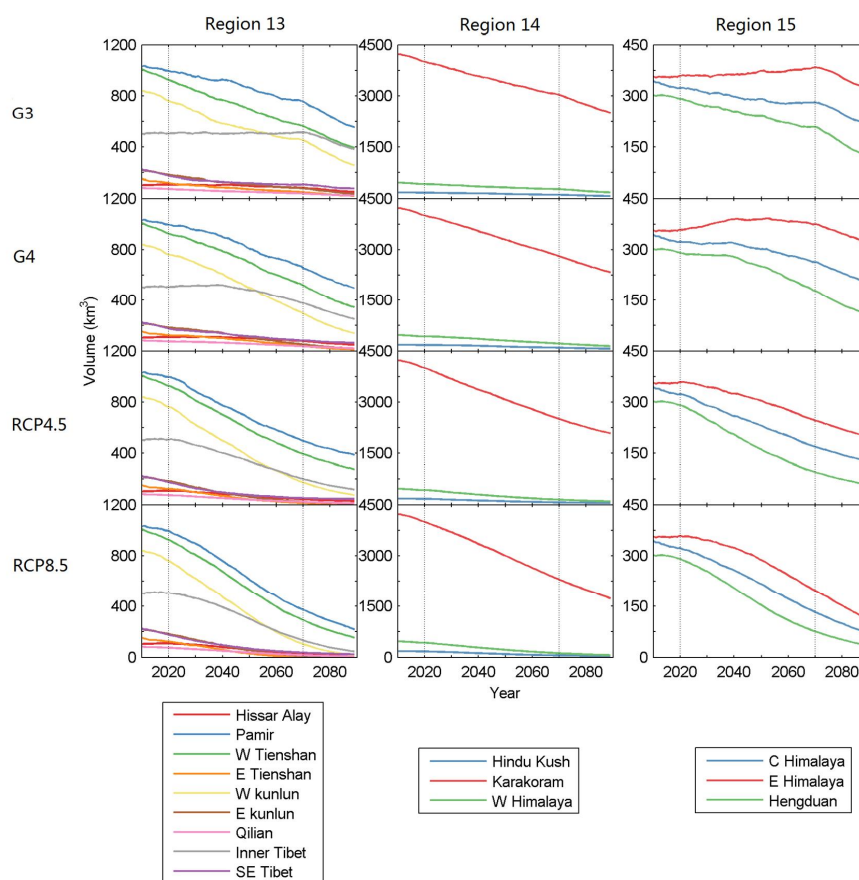


Fig. 7. Glacier volume (unit:  $\text{km}^3$ ) change from 2010 to 2089 for glaciers in sub-regions  
 of Region 13 (left column), 14 (middle column) and 15 (right column) under scenarios  
 300 by row from G3 (top), G4, RCP4.5, to RCP8.5 (bottom). The curves for sub-regions  
 are colour-coded in the legend.

#### 4.4 Uncertainties in projections

There are several uncertainties in this study. Firstly, there only 3 ESMs participated in  
 305 G3 than in G4 simply because doing the G3 experiment is difficult and time-consuming  
 to set-up. So the ensemble climate projection is less robust in G3 than in G4. Secondly,



although the goal of geoengineering schemes is to mitigate temperature warming, it inevitably also alters other important climate parameters, such as precipitation. We do not consider the impact of precipitation change on glacier change in this study, as the climate models do not simulate significant precipitation changes in the HMA region (Table 3). However, there will be generally less precipitation under geoengineering scenarios that balance long wave greenhouse gas radiative forcing with short wave forcing than under the RCP4.5 or RCP8.5 scenarios (Tilmes et al., 2013), which would be expected to lead to increased ice loss. So potentially our estimates of glacier wastage under G3 and G4 scenarios may be under-estimated. Simulating change in the Asian monsoon is difficult for climate models under geoengineering since the deep convection involved may also be influenced by chemistry changes in the stratosphere caused by the injected aerosols – most of the ESM models in our study do not have sophisticated aerosol chemistry schemes (though the MIROC-ESM-CHEM model does). Thirdly, we note that the distribution of meteorological stations in the study region is very sparse, especially in the northwest of this region (Liu and Chen, 2000). Therefore, both the Berkeley gridded data and temperature data from models projections that we used in this study may have low accuracy for specific glacier regions.

There are several key parameters in our algorithm which influence the modeled glacier volume loss and were summarized in Zhao et al. (2016). Here we consider the uncertainty resulting from using different initial ELA at the start year, different V-A scaling parameters and the effect of ELA sensitivity to precipitation.

For the initial ELAs for each glacier, several alternative choices are reasonable: we can use the ELA interpolated from the first Chinese glacier inventory, or median elevations from RGI dataset, or the elevation of the 60th percentile of the cumulative area above the glacier terminus (Zhao et al., 2016). These three choices lead to a range with coefficient of variation of 13% in glacier volume loss. In this study, we use median elevations from RGI dataset, which corresponds to the median result.

Including an ELA-precipitation sensitivity prescribed from Rupper and Roe (2008) and annual precipitation change rates over the period 1980-2050 from a high resolution regional model RegCM3 (Gao et al., 2012) forced by the IPCC A1B greenhouse gas



scenario leads to a reduced glacier loss of about 12% (Zhao et al., 2016) compared with rates when driven by temperature forcing alone. This is because most greenhouse gas forcing scenarios produce slight increases in precipitation over the HMA (Fig. 3). Here  
340 we do not take ELA sensitivity to precipitation into account and Table 3 suggests no reason to expect significant changes in precipitation across the region under either geoengineering or RCP scenarios.

Analysis by Zhao et al. (2014) showed that different volume-area scaling parameterizations can lead to  $\pm 5\%$  range of glacier volume loss. The set of parameters  
345 we use in this study corresponds to the lower bound of estimate, but one that is best matched to observational data. Combining the above three uncertainties would require a Monte Carlo simulation since the parameters combine non-linearly to produce glacier volume and area change; this is prohibitively expensive to perform given that a single simulation of all glaciers in HMA requires about 60 cpu hours on an 8 core computer  
350 with parallel computing in Matlab. We can illustrate the uncertainty range by assuming parameter errors are independent and ignore inherent non-linearity, which leads to an uncertainty range of about  $\pm 18\%$  in glacier volume losses (Fig. 6).

One further key parameter is the ELA sensitivity to summer mean temperature. Here we use the zonal mean values from energy-balance modelling of glaciers in HMA by  
355 Rupper and Roe (2008). Alternatively, it can be estimated using an empirical formula for ablation and a degree-day method (Zhao et al., 2016). However, we prefer the Rupper and Roe model estimates since the simulated variation in ELA over time using their ELA sensitivities to summer mean temperature fit best with observed time series of ELA decadal trends on nine glaciers (Zhao et al., 2016).

360

## 5 Conclusion

We project glacier volume loss, in equivalent sea-level rise, for all the glaciers from 2010 to 2089 as 18 mm and 21 mm under the RCP 4.5 and RCP8.5 scenarios, respectively. The volume change of all the glaciers in HMA over the 21th century  
365 estimated by Radić et al. (2014) is about  $15\pm 5$  mm under RCP4.5 and  $22\pm 5$  mm under RCP8.5. Marzeion et al. (2012) estimate about  $15.4\pm 4.5$  mm under RCP4.5, and



18.8±4.0 mm under RCP8.5 using projected temperature and precipitation anomalies from an ensemble of 15 CMIP5 climate models. These estimates are close to ours, despite their methodology being quite different from ours.

370 Terminating G3 geoengineering at 2069 leads to a rapid temperature rise and immediate increase in glacier reduction, with volume loss rates exceeding those from RCP8.5. Furthermore even the most extreme geoengineering (G3) only slows glacier shrinkage by about 50% relative to losses from RCP8.5 (8.4 and 16.8 mm sea level equivalent at 2069 respectively). Approximately 65% of glaciated area remains at 2069  
375 under G3 compared with about 35% for RCP8.5. The reason for the G3 losses is likely to be that the glaciers in HMA are not in equilibrium with present day climate, so simply stabilizing temperatures at early 21<sup>st</sup> century levels does not preserve them. To do that would require significant cooling, perhaps back to early 20<sup>th</sup> century levels. The 5 Tg of SO<sub>2</sub> per year specified in G4 is about the same loading as a 1991 Mount Pinatubo  
380 volcanic eruption every 4 yr (Bluth et al., 1992). G3 requires increasing rates of injection, to 9.8 Tg for the BNU-ESM at 2069. As aerosol loading increases, its efficacy decreases as particles coalesce and fall out of the stratosphere faster, while also becoming radiatively less effective (Niemeier and Timmreck, 2015). Thus it seems that the disappearance of at least 1/3 of the glaciated area in HMA by 2069 cannot be  
385 prevented by sulphate aerosol geoengineering.

### Acknowledgements

This study is supported by National Key Science Program for Global Change Research (2015CB953601), and National Natural Science Foundation of China (No. 41530748,  
390 41506212, 40905047).

### References

- Arendt, A., et al.: Randolph Glacier Inventory - A Dataset of Global Glacier Outlines: Version 5.0. (GLIMS Technical Report) Global Land Ice Measurements from  
395 Space, Boulder CO. Digital media, 2015.
- Arora, V.K., et al.: Carbon emission limits required to satisfy future representative concentration pathways of greenhouse gases, *Geophys. Res. Lett.*, 38(5), L05805,



- 2011.
- 400 Azam, M.F., Wagnon, P., Ramanathan, A., Vincent, C., Sharma, P., Arnaud, Y., Linda, A., Pottakkal, G.J., Chevallier, P., Singh, V.B., and Berthier, E.: From balance to imbalance: a shift in the dynamic behaviour of Chhota Shigri Glacier (Western Himalaya, India), *J. Glaciol.*, 58 (208), 315–324, 2012.
- 405 Applegate, P.J. and Keller, K.: How effective is albedo modification (solar radiation management geoengineering) in preventing sea-level rise from the Greenland Ice Sheet? *Environ. Res. Lett.*, 10, 084018, 2015.
- Bluth, G.J.S., Doiron, S.D., Schnetzler, C.C., Krueger, A.J., and Walter, L.S.: Global tracking of the SO<sub>2</sub> clouds from the June 1991 Mount Pinatubo eruptions, *Geophys. Res. Lett.*, 19, 151–154, 1992.
- 410 Collins, W.J., et al.: Development and evaluation of an earth-system model-HadGEM2, *Geoscience Model Development*, 4, 1051–1075, 2011.
- Dufresne, J.-L., et al.: Climate change projections using the IPSL-CM5 earth system model: From CMIP3 to CMIP5, *Clim. Dyn.*, 40, 2123–2165, 2013.
- Du, J., He, Y., Li, S., Wang, S., Niu, H., Xin, H., and Pu, T.: Mass balance and near-surface ice temperature structure of Baishui Glacier No.1 in Mt. Yulong, *Journal of Geographical Sciences*, 23 (4), 668–678, 2013.
- 415 Gao, X., Shi, Y., Zhang, D., and Giorgi, F.: Climate change in China in the 21st century as simulated by a high resolution regional climate model, *Chin. Sci. Bull.*, 57, 1188–1195, 2012.
- 420 Irvine, P.J., Lunt, D.J., Stone, E.J., and Ridgwell, A.J.: The fate of the Greenland Ice Sheet in a geoengineered, high CO<sub>2</sub> world, *Environ. Res. Lett.*, 4, 045109, 2009.
- Irvine, P.J., Sriver, R.L., and Keller, K.: Tension between reducing sea-level rise and global warming through solar radiation management, *Nat. Clim. Change*, 2, 97–100, 2012.
- 425 Ji, D., et al.: Description and basic evaluation of Beijing Normal University Earth System Model (BNU-ESM) version 1, *Geoscientific Model Development*, 7, 2039–2064, 2014.
- 430 Jones, A., Haywood, J.M., Alterskjaer, K., Boucher, O., Cole, J.N.S., Curry, C.L., Irvine, P.J., Ji, D., Kravitz, B., Kristjánsson, J.E., Moore, J.C., Niemeier, U., Robock, A., Schmidt, H., Singh, B., Tilmes, S., Watanabe, S., and Yoon, J.-H.: The impact of abrupt suspension of solar radiation management (termination effect) in experiment G2 of the Geoengineering Model Intercomparison Project (GeoMIP), *J. Geophys. Res. Atmos.*, 118 (17), 9743–9752, 2013.
- 435 Kravitz, B., A. Robock, O. Boucher, H. Schmidt, K. E. Taylor, G. Stenchikov, and M. Schulz, The Geoengineering Model Intercomparison Project (GeoMIP), *Atmos. Sci. Lett.*, 12(2), 162–167, 2011.
- Liu, X. and Chen, B.: Climatic warming in the Tibetan Plateau during recent decades, *Int. J. Climatol.* 20: 1729–1742, 2000.
- Marzeion, B., Jarosch, A.H., and Hofer, M.: Past and future sea-level change from the surface mass balance of glaciers, *Cryosphere* 6, 1295–1322, 2012.
- 440 McCusker, K.E., Battisti, D.S., and Bitz, C.M.: Inability of stratospheric sulfate aerosol injections to preserve the West Antarctic Ice Sheet, *Geophys. Res. Lett.*, 42, 4989–



- 4997, 2015.
- Mölg, T., Maussion, F., Yang, W., and Scherer, D.: The footprint of Asian monsoon dynamics in the mass and energy balance of a Tibetan glacier, *Cryosphere* 6, 1445–1461, 2012.
- 445 Moore, J.C., Jevrejeva, S., and Grinsted, A.: Efficacy of geoengineering to limit 21st century sea-level rise, *Proc. Natl. Acad. Sci.*, 107, 15699–15703, 2010.
- Niemeier, U. and Timmreck, C.: What is the limit of stratospheric sulfur climate engineering? *Atmos. Chem. Phys. Discuss*, 15, 10939–10969, 2015.
- 450 Pu, J., T. Y., Duan, K., Sakai, A., Fujita, K., and Matsuda, Y.: Mass balance of the Qiyi Glacier in the Qilian Mountains: a new observation (in Chinese with English abstract), *J. Glaciol. Geocryol.* 27, 199–204, 2005.
- Ricke, K.L., Morgan, M.G., and Allen, M.R.: Regional climate response to solar-radiation management, *Nat. Geosci.*, 3, 537–541, 2010.
- 455 Radić, V., Bliss, A., Beedlow, A.C., Hock, R., Miles, E., and Cogley, J.G.: Regional and global projections of the 21st century glacier mass changes in response to climate scenarios from GCMs. *Clim. Dyn.*, 42, 37–58, 2014.
- Rupper, S. and Roe, G.: Glacier changes and regional climate: a mass and energy balance approach, *J. Clim.*, 21, 5384–5401, 2008.
- 460 Taylor, K.E., Stouffer, R.J., and Meehl, G.A.: An overview of CMIP5 and the experiment design, *Bulletin of the American Meteorological Society*, 93, 485–498, 2012.
- Tilmes, S., et al.: The hydrological impact of geo-engineering in the Geoengineering Model Intercomparison Project (GeoMIP), *J. Geophys. Res.*, 118(19), 11036–11058, 2013.
- 465 Wagnon, P., Linda, A., Arnaud, Y., Kumar, R., Sharma, P., Vincent, C., Pottakkal, G.J., Berthier, E., Ramanathan, A., Hasnain, S.I., and Chevallier, P.: Four years of mass balance on Chhota Shigri Glacier, Himachal Pradesh, India, a new benchmark glacier in the Western Himalaya, *J. Glaciol.*, 53 (183), 603–610, 2007.
- 470 Wang S., Pu J., and Wang N.: Study of Mass Balance and Sensibility to Climate Change of Qiyi Glacier in Qilian Mountains (in Chinese with English abstract), *J. Glaciol. Geocryol.*, 33(06), 1214–1221, 2011.
- Watanabe, S., et al.: MIROC-ESM 2010: Model description and basic results of CMIP5-20c3m experiments. *Geoscience Model Development* 4, 845–872, 2011.
- 475 WGMS: Glacier Mass Balance Bulletin No. 1 (1988-1989), ed. Haeberli, W., and E. Herren. IAHS (ICSU)/UNEP/UNESCO, World Glacier Monitoring Service, Zurich, 1991.
- WGMS: Glacier Mass Balance Bulletin No. 2 (1990-1991), ed. Haeberli, W., E. Herren and M. Hoelzle. IAHS (ICSU)/UNEP/UNESCO, World Glacier Monitoring Service, Zurich, 1993.
- 480 WGMS: Glacier Mass Balance Bulletin No. 3 (1992-1993), ed. Haeberli, W., M. Hoelzle and H. Bosch. IAHS (ICSU)/UNEP/UNESCO, World Glacier Monitoring Service, Zurich, 1994.
- WGMS: Glacier Mass Balance Bulletin No. 4 (1994-1995), ed. Haeberli, W., M. Hoelzle and S. Suter. IAHS (ICSU)/UNEP/UNESCO, World Glacier Monitoring
- 485



- Service, Zurich, 1996.
- WGMS: Glacier Mass Balance Bulletin No. 5 (1996-1997), ed. Haeberli, W., M. Hoelzle and R. Frauenfelder. IAHS (ICSU)/UNEP/UNESCO, World Glacier Monitoring Service, Zurich, 1999.
- 490 WGMS: Glacier Mass Balance Bulletin No. 6 (1998-1999), ed. Haeberli, W., R. Frauenfelder and M. Hoelzle. IAHS (ICSU)/UNEP/UNESCO/WMO, World Glacier Monitoring Service, Zurich. WGMS. 2003. Glacier Mass Balance Bulletin No. 7 (2000-2001), ed. Haeberli, W., R. Frauenfelder, M. Hoelzle and M. Zemp. IAHS (ICSU)/UNEP/UNESCO/WMO, World Glacier Monitoring Service, Zurich,
- 495 2001.
- WGMS: Glacier Mass Balance Bulletin No. 8 (2002-2003), ed. Haeberli, W., J. Noetzli, M. Zemp, S. Baumann, R. Frauenfelder and M. Hoelzle. IUGG (CCS)/UNEP/UNESCO/WMO, World Glacier Monitoring Service, Zurich, 2005.
- 500 WGMS: Glacier Mass Balance Bulletin No. 9 (2004-2005), ed. Haeberli, W., M. Hoelzle and M. Zemp. ICSU (FAGS)/IUGG (CCS)/UNEP/UNESCO/WMO, World Glacier Monitoring Service, Zurich, 2007.
- WGMS: Glacier Mass Balance Bulletin No. 10 (2006-2007), ed. Haeberli, W., I. Gärtner-Roer, M. Hoelzle, F. Paul and M. Zemp. ICSU (WDS)/IUGG (IACS)/UNEP/UNESCO/WMO, World Glacier Monitoring Service, Zurich, 2009.
- 505 WGMS: Glacier Mass Balance Bulletin No. 11 (2008-2009), ed. M. Zemp, S. U. Nussbaumer, I. Gärtner-Roer, M. Hoelzle, F. Paul and W. Haeberli. ICSU (WDS)/IUGG (IACS)/UNEP/UNESCO/WMO, World Glacier Monitoring Service, Zurich, 2011.
- WGMS: Glacier Mass Balance Bulletin No. 12 (2010-2011), ed. M. Zemp, S. U. Nussbaumer, K. Naegeli, I. Gärtner-Roer, F. Paul, M. Hoelzle and W. Haeberli. ICSU (WDS)/IUGG (IACS)/UNEP/UNESCO/WMO, World Glacier Monitoring Service, Zurich, 2013.
- 515 Yang, W., Yao, T., Guo, X., Zhu, M., Li, S., and Kattel, D. B.: Different region climate regimes and topography affect the changes in area and mass balance of glaciers on the north and south slopes of the same glacierized massif (the West Nyainqentanglha Range, Tibetan Plateau), *Journal of Hydrology* 495, 64-73, 2013.
- Yao, T., Thompson, L., Yang, W., Yu, W., Gao, Y., Guo, X., Yang, X., Zhao, H., Duan, K., Xu, B., Pu, J., Lu, A., Qin, D.H., Xiang, Y., Kattel, D.B., and Joswiak, D.: Different glacier status with atmospheric circulations in Tibetan Plateau and surroundings, *Nat. Clim. Chang.* 15, 2012, <http://dx.doi.org/10.1038/NCLIMATE1580> (supplementary information).
- 520 Yang, W. and T. Yao, et al.: Mass balance of a maritime glacier on the southeast Tibetan Plateau and its climatic sensitivity, *J. Geophys. Res. Atmos.*, 118 (17), 9579-9594, 2013.
- 525 Yu, X., Moore, J. C., Cui, X., Rinke, A., Ji, D., Kravitz, B. and Yoon J.-H.: Impacts, effectiveness and regional inequalities of the GeoMIP G1 to G4 solar radiation management scenarios, *Global Planet. Change*, 129, 10–22, 2015.
- Zhang, J., He, X., Ye, B., et al.: Recent Variation of Mass Balance of the Xiao Dongkemadi Glacier in the Tanggula Range and its influencing factors (in Chinese



- 530 with English abstract), *J. Glaciol. Geocryol.*, 35(2), 263-271, 2013.
- Zhang, H., Li, Z., Wang, P., and Huai, B.: Variation of Haxilegen No.51 Glacier at the Headwater of Kuytun River in Tianshan Mountains and Its Response to Climate Change, *Arid Zone Research*, 32(1), 88-93, 2015.
- 535 Zhou, G., Yao, T., Kang, S., Pu, J., Tian, L., and Yang, W.: Mass balance of the Zhadang Glacier in the central Tibetan Plateau (in Chinese with English abstract). *J. Glaciol. Geocryol.* 29 (3), 360–365, 2007.
- Zhao, L., Ding, R., and Moore, J.C.: Glacier volume and area change by 2050 in high mountain Asia, *Global Planet. Change*, 122, 197-207, 2014.
- Zhao, L., Ding, R., and Moore, J.C.: The High Mountain Asia glacier contribution to  
 540 sea level rise from 2000 to 2050, *Ann. Glaciol.*, 71, 223-231, 2016.

Table 1. The benchmark glaciers.

Glacier name	Sub-region	Location	Averaged SMB gradients	Period of SMB measurements	Reference
Abramov Glacier	13-01	(39°38'N, 71°36'E)	0, z>ELA+200; 0.0088, z<ELA+200.	1987-1997	Glacier mass balance bulletin No. 1-6.
Ts. Tuyuksuyskiy Glacier	13-03	(43°03'N, 77°05'E)	0, z>ELA+100; 0.0057, z<ELA+100.	1987-2011	Glacier mass balance bulletin No. 1-12.
Urumqihe S. No.1 Glacier (East branch)	13-04	(43°06'N, 86°49'E)	0.002, ELA<z<4300; 0.01, z<ELA.	1987-2011	Glacier mass balance bulletin No. 1-12.
Haxilegen No.51 Glacier	13-04	84°24'E, 43°43'N	0.012	1999-2005	Zhang et al. (2015)
Qiyi Glacier	13-07	(39°14'N, 97°45'E)	0.0042, 4800<z<ELA; 0.0014, z<4800.	2002 Jun-Sep; 2002-03; 2010	Pu et al. (2005); Wang et al.(2011)
Zhadang Glacier	13-08	(30°28'N, 90°38'E)	0.0041	2005-06; 2009 Jun-Jul; 2009 Sep-2010May; 2010 Aug-Sep	Zhou et al.(2007), Mølg et al. (2012), Yu et al. (2013)
Gurenhekou Glacier	13-08	(30°11'N, 90°27'E)	0.0041	2004-08	Yu et al. (2013)
Xiao Dongkemadi Glacier	13-08	(33°04'N, 92°05'E)	0.007, z<ELA; 0.004, ELA<z<5750	2008-12	Zhang et al. 2013)
Chhota Shigri Glacier	14-03	(32°12'N, 77°30'E)	0.003, ELA<z<5600; 0.01, ELA-150<z<ELA; 0.005, 4000<z<ELA-150	Annual average SMB during 2002-10; 2003-04; 2004-05	Azam et al. (2012); Wagnon et al. (2007)



Naimona'nyi Glacier	15-01	(30°27'N, 81°20'E)	0.0006, z>ELA; 0.0038, 5700<z<ELA;	2005-2010	Yao et al. (2012)
Kangwure Glacier	15-01	(28°28'N, 85°49'E)	0.0038, 5700<z<6100;	2005-2010	Yao et al. (2012)
Parlung No.94 Glacier	15-03	(29°20'N, 97°0'E)	0.01	2006-10	Yang et al. (2013)
Baishui No.1 Glacier	15-03	26°59'–27° 17'N, 100°04'–10 0°15'E	0.003, z>ELA 0.01, ELA-250<z <ELA; 0.0035, 4300<z<4650	2008-09	Du et al. (2013)

545

Table 2 Gridded climate data sets used in this study.

Name	Reference	Resolution	Data sets
<b>Berkeley Earth project</b>	Rohde et al., 2013	1°× 1°	Surface temperature 1980-2013
<b>BNU-ESM</b>	Ji et al., 2014	2.8°× 2.8°	G3,G4, RCP4.5, RCP8.5
<b>CanESM2</b>	Arora et al., 2011	2.8°× 2.8°	G4, RCP4.5, RCP8.5
<b>HadGEM2-ES</b>	Collins et al., 2011	1°× 1.9°	G3,G4, RCP4.5, RCP8.5
<b>IPSL-CM5A-LR</b>	Dufresne et al., 2013	1.9°× 3.8°	G3, RCP4.5, RCP8.5
<b>MIROC-ESM</b>	Watanabe et al., 2011	2.8°× 2.8°	G4, RCP4.5, RCP8.5
<b>MIROC-ESM-CHEM</b>	Watanabe et al., 2011	2.8°× 2.8°	G4, RCP4.5, RCP8.5

550 Table 3. Mean and standard deviation of mean surface air temperature and precipitation anomalies averaged over the whole study region during 2030–2069 simulated from G3, G4, RCP4.5 and RCP8.5 ensembles (Table 2). Anomalies are relative to the baseline RCP4.5 climate state between 2010 and 2029.

Ensemble	$\Delta T$ (°C)	$\Delta P$ (mm day <sup>-1</sup> )
<b>G3</b>	0.17±0.18	0.01±0.07
<b>G4</b>	0.50±0.34	0.05±0.08
<b>RCP4.5</b>	1.30±0.34	0.07±0.10
<b>RCP8.5</b>	2.03±0.46	0.09±0.13